Computed Tomography

12

Jürgen Goebbels

12.1 Principle

Computed tomography (CT) with X- and Gamma-rays is a well-known imaging method, established first for medical use [1]. Applications to non-destructive testing were published in the early 1980s [2]. CT offers the possibility to map non-invasively the three-dimensional local absorption of X-rays of samples and components, which correspond to the inner and outer structures. The result of a CT measurement is usually given in the form of a 3D image matrix. Each point represents a single volume element in the sample, a voxel. CT delivers an absolute measure, the linear attenuation coefficient μ, for the absorbed X-ray radiation averaged over one voxel. Depending on the sample diameter, the maximum material thickness which has to be penetrated and the used equipment, details as small as a few μm, can be characterised and resolved [3]. With Synchrotron CT with their advantage of parallel beam and high photon flux even at monochromatic energies, these limits are at present in the nanometre range [4–6].

12.2 Scanning Methods and Reconstruction Algorithms

Generally the samples have to be irradiated from all directions, i.e. over 360°. For special applications a reduced set of projections can be used. The terms for this are 'Limited angle CT', 'Laminography', etc. [7, 8].

Depending on the applied scanning method different reconstruction algorithms can be applied [9]. The most used algorithm is the filtered back projection algorithm for single slice CT and fan beam geometry and its extension to cone beam tomography, the Feldkamp-David-Kress (FDK) algorithm [10]. The known expansions are the Spiral-CT, first developed for medical CT with line detectors [11]. Using flat panel detectors Spiral-CT [12, 13] allows to overcome the limitations of the FDK algorithm, which is an approximation valid only for small opening angles of the X-ray cone beam. In the following only results of complete scanning CT are described.

12.3 Applications

The main applications of CT handled extensively in this chapter are: density distribution and material composition, porosity and porosity distribution, flaws and related properties, fibre reinforced materials, corrosion phenomena and dimensional control.

J. Goebbels (✉)
Bundesanstalt für Materialforschung und–prüfung, Unter den Eichen 87, 12205 Berlin, Germany
e-mail: juergen.goebbels@t-online.de

Fig. 12.1 *Green* alumina component. *Right side* flaws and density or porosity gradients in radial and axial intersection. *Left side* density scale
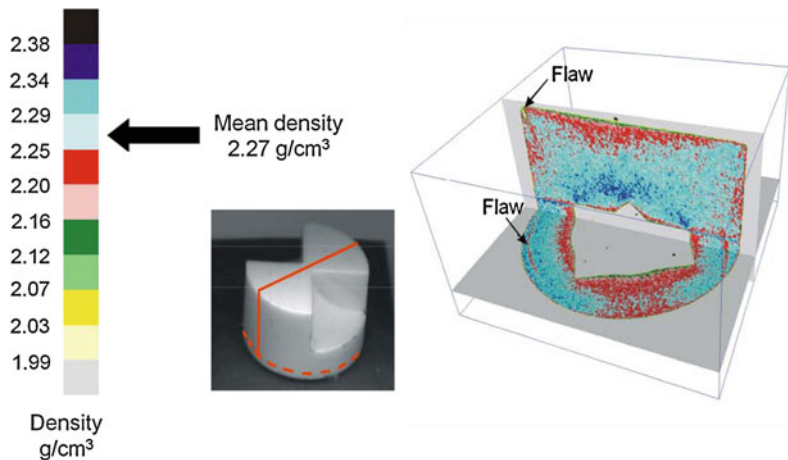
12.4 Density Distribution

The advantage of non-destructive methods is that such methods can be applied to sensitive components like green state ceramics. CT is the only method which gives information about the 3D density distribution in such samples. With CT it is possible to determine green-body density variations with high local resolution even in complex-shaped components. Density gradients caused by shaping process, the influence of press parameters, irregular filling conditions or changes in the moisture content of the granules are only a few examples which can be detected, quantified and used for an optimised production process.

The first experiments with 2D CT were done by investigating ceramic samples [14]. Using Cone beam CT together with a very careful calibration of the CT system a lot of work was done [15, 16], including a comparison with theoretical calculations.

As an example, a green alumina component is shown in Fig. 12.1. It has a diameter of 19 mm, a height of 12 mm and a mean density of 2.27 g/cm^3 corresponding to a mean porosity of about 43 %. The coloured absolute density scale is related to the mean density. The complex shape shows high and low density regions. Flaws can also be detected presumably caused by the ejection process.

12.5 Porosity Size and Distribution

If the pores can be resolved and classified the pore size distribution can be determined together with analysing open and closed porosity [17, 18]. Especially for cellular materials like plastics or aluminium foam, much information can be extracted from CT measurement such as pore size distribution, number of nodes, wall thickness parameters and other structural parameters that define the properties of such materials [19].

12.6 Material Composition

With CT a biunique determination of chemical composition of a material is usually not possible due to the fact that the X-ray absorption is a mixture of electron density and physical density. Some efforts are done using more advanced techniques like dual-energy CT [20, 21], X-ray fluorescence tomography (mainly used in connection with synchrotron radiation) and other methods to reduce this limitation. However, these methods cannot be applied generally due to the essential dependence of these methods on the sample size, material combination and X-ray energies. For materials with phases which differ well in the absorption an analysis of the composition of the samples can be performed from classical CT image data sets only.

Fig. 12.2 Two slices of the 3D-data set of two core samples ($\varnothing = 50$ mm, height = 40 mm). The sample at right was contaminated artificially with dust
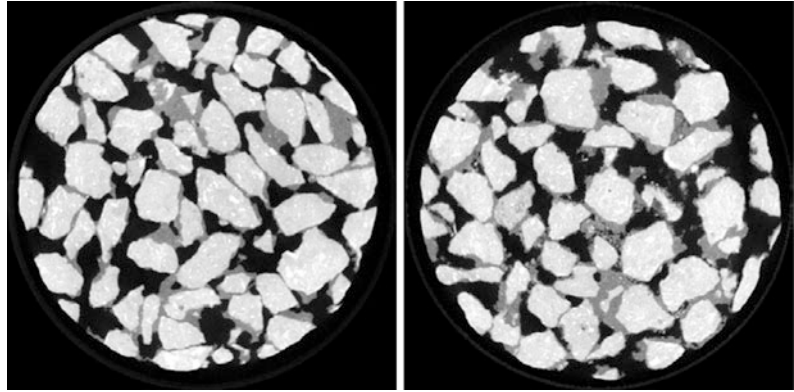
Open porous asphalt, which is used to reduce traffic noise, is such a system [22]. It is an open graded mixture of coarse and fine aggregates, mineral filler and a bituminous-based binder, with air voids greater than 25 %. In practice, when the open porous asphalt is in use on streets, the dust infiltration is added. To characterise the properties a number of samples from laboratory experiments and from core samples extracted from roads are investigated to determine the content of bitumen/binder, of coarse aggregates and air before tests are performed with dusty samples [23]. Other morphological features like grain size distribution, open or closed porosity and pore size distribution can be extracted from CT measurements to characterise the properties of these materials.

Figure 12.2 shows an example of two open porous bitumen core samples together with the histogram (see Fig. 12.3) belonging to it. Due to the selected spatial resolution—voxel size 52 μm—appropriate for such core samples, the
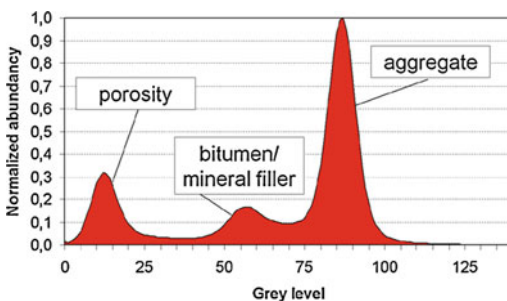
two phases bitumen/filler and dust appears not to be separated in the histogram. The ratio of phases for the left image in Fig. 12.2 is 16.3 ± 0.2 % bitumen/mineral filler, 57.7 ± 0.3 % aggregate and 26.0 ± 0.3 % air/porosity.

12.7 Flaw Analysis

The classical use of CT in NDT is the detection and classification of flaws, pores, shrink holes and discontinuities. Especially the size and the precise location of flaws can be determined with CT. This behaviour is also used to calibrate other NDT methods like Eddy current and Ultrasonic Techniques. There are many publications about the detection of flaws with CT [24].

A challenge is the precise quantification of defect size. A method for obtaining quantitative information in 3D on CT's ability to measure the geometry and to detect defects is to measure calibrated test pieces (reference standards) and defect detection [25]. To obtain a test piece with inner geometries measured by tactile means, a small aluminium cylinder head was divided into four pieces in such a way that the innermost surfaces can be reached with a tactile probe (Fig. 12.4). Reference geometries (spheres and cylinders) were applied to define a coordinate system for aligning the measurements in the disassembled and reassembled states. The four pieces were reassembled after the tactile measurement.

The test piece also contains casting defects. In order to be able to use the assembled cylinder head as reference sample for defect detection,
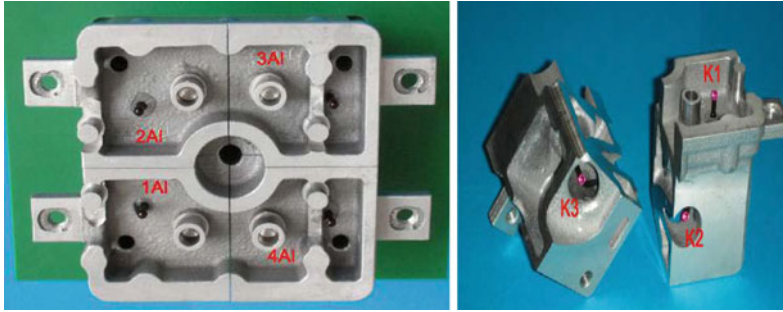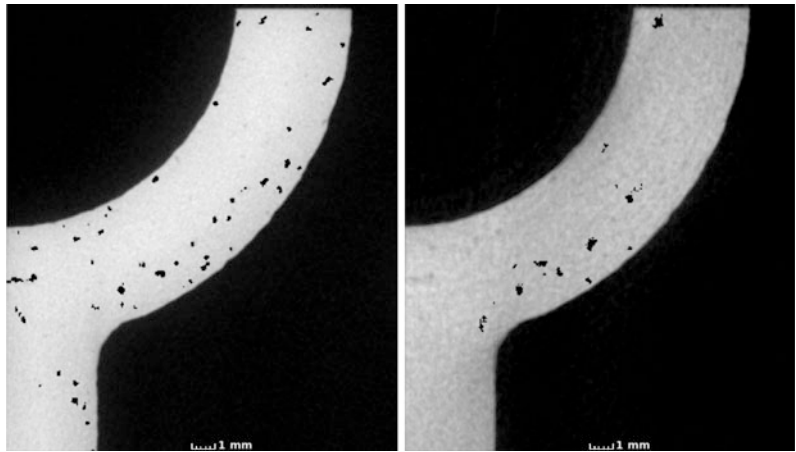

Fig. 12.3 Histogram analysis of content of a bitumen sample

Fig. 12.4 Mini cylinder head no. 5, divided into four pieces, 1Al… 4Al (*left image*). Two segments of mini cylinder head no. 5 with the visible spheres (*right image*)

Fig. 12.5 The detected defects (*marked black*) in the averaged reference data (*left*) and in the assembled cylinder head measurement (*right*)

measurements with higher spatial resolution and better signal-to-noise ratio were performed on the single parts (Fig. 12.5). For improving the reliability of the reference measurements, CT measurements of each part were carried out in three different orientations, and the individual defect detections were combined to obtain a reference data set with a high probability of defect detection and a low rate of erroneous detections. This new method for comparing the defect detection in a CT measurement to a reference data set demonstrates individual information about every detected flaw.

An alternative method to quantify precisely flaws in real components is the simultaneous measurement of a test piece with well-defined flaws. As an example a cube of a volume of 1 cm^3 was constructed, composed of monocrystalline Si plates (thickness 0.5 and 1 mm) with well-defined flaws. The flaws have a diameter between 50 and 1,000 μm.

Figure 12.6 represents a 3D visualisation of this test piece. In the well-defined flaws, the dimensions determined by other methods are marked red [26]. The advantage of using monocrystalline Si is its homogeneity and an X-ray absorption coefficient appropriate to aluminium castings.

12.8 Fibre Reinforced Materials

The knowledge of fibre distribution and orientation, fibre density and volume content, order parameter, fibre cracks and fibre arrangement is essential for properties of materials such as fibre reinforced concrete, fibre reinforced plastics, fibre reinforced carbon, metal matrix composites (MMC) and other materials containing fibres, including paper. Different approaches exist to extract information from the CT volume data set
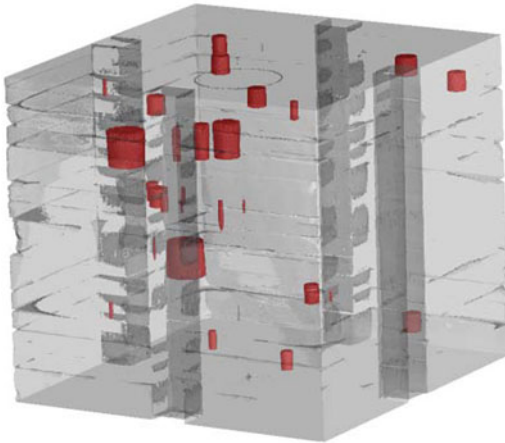
Fig. 12.6 Test piece, composited from smaller parts with well-defined flaws

about such features. Statistical methods as well as single fibre extractions are developed and applied for characterisation [27–29].

As an early example in the framework of the building activities at Potsdamer Platz in Berlin, steel fibre concrete for underwater slabs were used and core samples of fibre reinforced concrete were tested at BAM [30, 31]. Figure 12.7 gives some results, showing samples with low/high content of fibres as well as with oriented and randomly distributed fibres.

An example for a statistical analysis is given for the production process of fibre reinforced autoclaved aerated concrete [32]. Hereby, a preferential orientation of fibres is induced. For better understanding of the development of the fibre arrangement during the foaming process of the concrete, digital radiography was used to study the evolution of orientation in situ. The strength and the deformation behaviour of this building material are largely influenced by the

fibre orientation. Therefore, information about the fibre orientation is highly desirable. CT allows a non-destructive study of fibre reinforced autoclaved aerated concrete on different scales with laboratory equipment. The contrast between fibres and concrete matrix is sufficiently high even for glass fibres. Two different ways to study the fibre orientation are compared. The results correlate with the strength and the deformation behaviour of the samples. A high resolution study of the fibre environment shows that the fibres align the adjacent pores. An analysis of fibre orientation requires a large amount of fibres. As fibre reinforced autoclaved aerated concrete contains only few volume percent fibres compared to fibre reinforced plastics, a large volume needs to be studied (i.e. a few centimetres' edge length). Fortunately the fibre geometry can be extracted reliably from CT image data with a voxel size larger than the smallest fibre dimension. To study the fibre environment in detail a higher resolution was used. CT measurements of highly structured samples of such size can be performed with laboratory set-ups at low expense allowing high sample numbers. The flat panel detectors used in recent CT set-ups allow digital radiography with high time resolution. This was used to study the evolution of orientation during the foaming of the concrete.

If fibres can be assumed to be long cylinders oriented freely in space their orientation can be determined from the cylinder end coordinates. Subsequent to a labelling these coordinates can be obtained easily for each single fibre with a self-written program. The labelling, i.e., the one-to-one assignment of each separated object in the CT image volume to a number and setting of
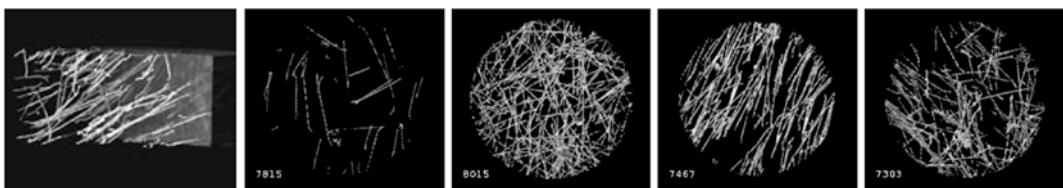

Fig. 12.7 Fibre reinforced concrete. Sample diameter 100 mm. Steel fibre diameter 0.6 mm, fibre length 50 mm, steel fibre reference input: 40 kg/m^3. The images show from *left to right* a 3D-visualisation of the analysed part of a core sample, a sample with low content of fibres, high content, oriented fibres and randomly distributed fibres
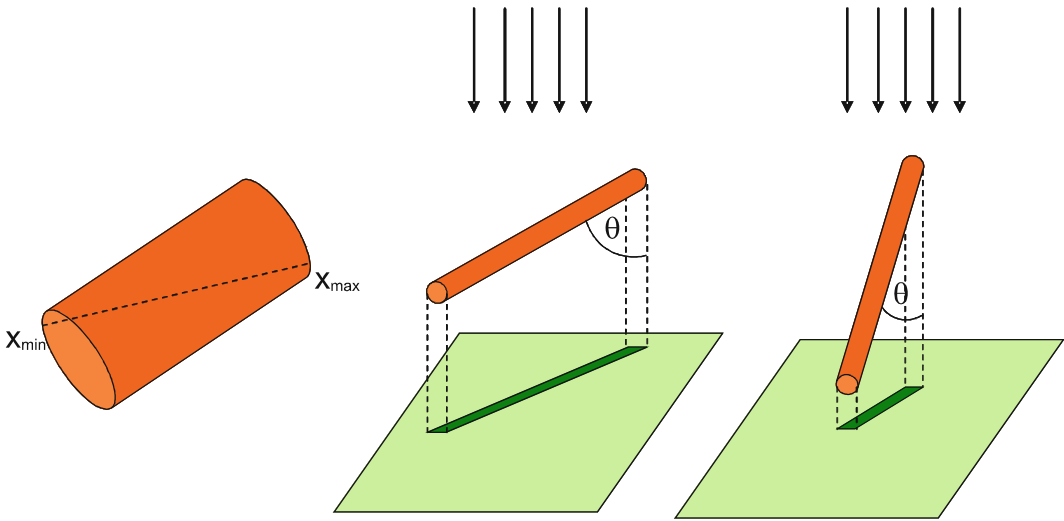
Fig. 12.8 *Left* the derivation of the fibre orientation and length from the maximum and minimum coordinates result in a faint deviation from cylinder axis. *Right* the area projected into a plain from a fibre is a function of the polar angle

its voxels' grey value to this number can be performed with software commercially available (for instance MAVI from Fraunhofer ITWM, or VG Studio Max from Volume Graphics). The self-written program determines for each grey value (i.e. each object) the minimum and maximum x, y, z coordinates as well as the residual coordinates belonging to each extreme. The coordinates of that pair of extrema with the highest absolute value of the difference are closest to the end point coordinates of the cylinder axis (see Fig. 12.8, left). Additionally, the choice of these coordinates is suited best to minimise the effects of a deviation from an ideal cylinder shape. As far as the length L of the fibre is much higher than its diameter D only faint
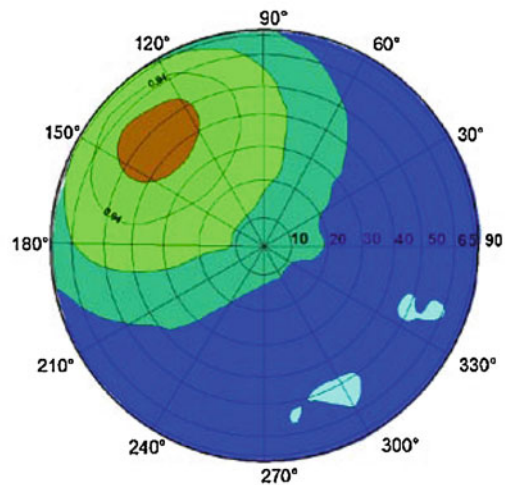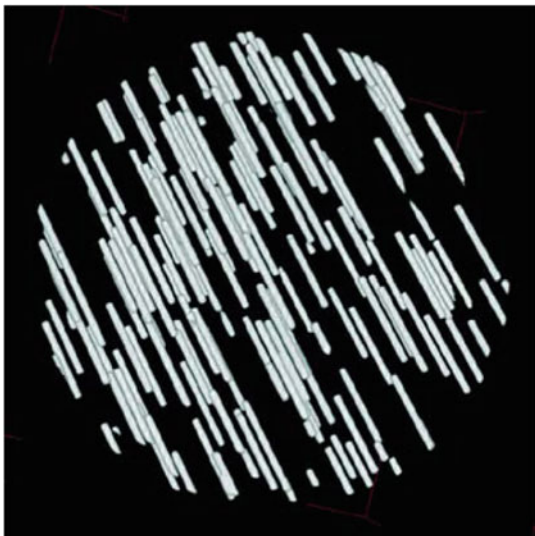

Fig. 12.9 *Left* 3D view of the model fibre dataset. *Right* Orientation distribution of the model dataset derived by projection. The normalised number of zero valued pixels in the projection is plotted into a stereographic projection. The azimuth is plotted circumferential, the polar angle radial

deviations from the real length (<1 % for L/D = 10) and orientation arise from this treatment. The maximum deviation for the angle amounts to 5.7° for L/D = 10 and 0.5° for L/D = 100. The latter is fulfilled for the bundled glass fibre of interest in this work. The orientation analysis from fibre end points provides the polar angle and the azimuth for each fibre. From that the total number or length of fibres per solid angle (steradian) can be calculated and plotted into a stereographic projection. The validity is tested with a model fibre set, shown in Fig. 12.9.

12.9 Corrosion

CT in general is not the favoured tool for the investigation of large structures like civil buildings. But it is a unique tool to study non-destructively time-dependent properties in smaller samples and to combine the results with other techniques, which are more suitable for large structures. As an example the study of self-corrosion was investigated [33, 34]. For the electrochemical investigations, mortar cylinders with embedded electrodes were produced (cylinder: height 120 mm, diameter 80 mm). The concrete cylinder simulates a constant concrete cover (35 mm). At the centre of the specimen a small steel cylinder (working electrode) welded to a stainless steel filler wire is fixed. The steel cylinder had a diameter of 9 mm, a height of 10 mm and a surface of 4.1 cm^2. In addition to the working electrode a counter electrode (platinised titanium net) was embedded.

Finally the results of the electrochemical studies and the results from the CT data—Figs. 12.10 and 12.11 show the embedded electrode at different stages of corrosion—were correlated to give a prognosis of the corrosion progress. The mass loss determined by electrochemical data and the mass loss calculated from CT data, extracting the electrode volume by image analysis was compared. The time dependence of mass loss is shown in Fig. 12.12. In addition, the differentiation between total and pitting corrosion is essential for the corrosion progress and was first shown in these investigations non-destructively by CT.

12.10 Dimensional Control

A characteristic of the samples is the dimension of components, especially the form and size. In the past 10 years the measurement and determination of geometric features with common coordinate measurement machines (CMM) was supported and expanded by CT as a new sensor. A lot of efforts were done to improve the uncertainty of the dimensional control with CT [35, 36], using well-designed test samples as the sample (see Fig. 12.4) which is used as a reference sample for flaw determination.

For the results reached with an uncertainty in the μ range, the dimensional control of a micro gear is described [37, 38]. Micro gears with an
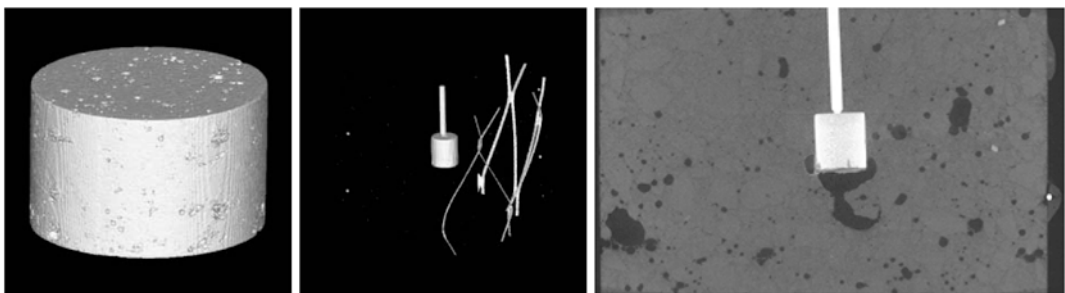

Fig. 12.10 Two iso-surface visualisations of the outer surface of the concrete sample (*left*) and the inner electrode together with the counter electrode (*middle*). Cross section of sample M1Cl4/26 (*right*)
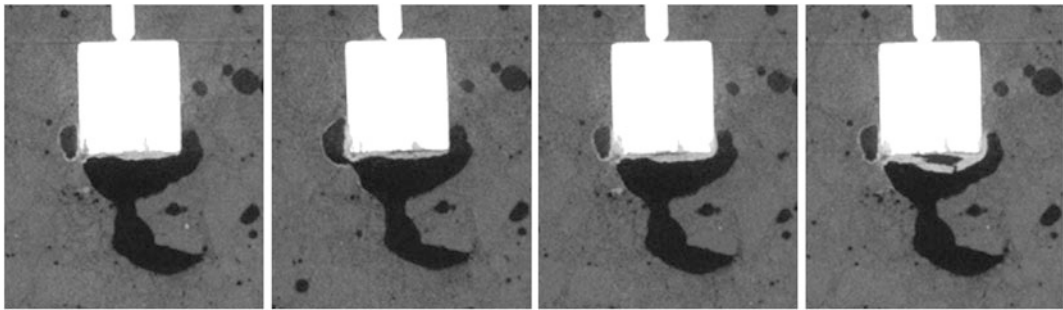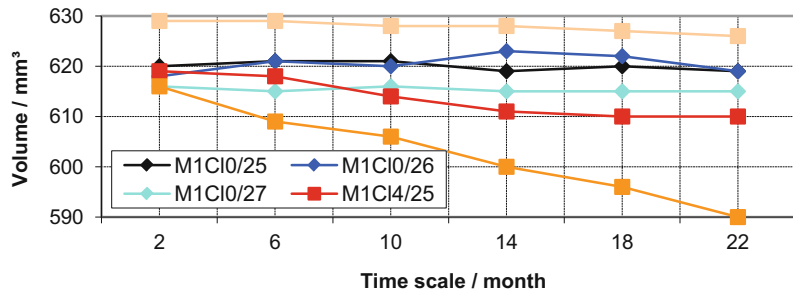
Fig. 12.11 Details of the electrode of a chloride concrete sample at different stages of self corrosion

Fig. 12.12 Volume reduction of electrode for two sets of samples as function of time

outer diameter of a few mm are often used in micro sun and planet gears. Figure 12.13 shows a micro gear made of steel with 14 teeth.

The micro CT measurements were performed using a CT system of BAM with 80 kV voltage, 0.25 mm Cu filtering, $(3.6 \ \mu m)^3$ voxel size and $2{,}048 \times 2{,}048$ pixel detector size. In total, six independent CT measurements were recorded.

Surface data was created from the CT volume data by an adaptive threshold process using Volume Graphics *Studio Max 2.02*. The quality of surfaces was levelled for optimal processing resulting in polygon data sets with 1.5 millions triangles for each set. The CT data was corrected for first order scaling errors by correcting the nominal voxel size with the known diameter of the core hole of the gear (assessed by tactile micro CMM measurements). The registration of the CT and of the tactile point data was accomplished step by step. The final alignment was performed by a restricted Gaussian best fit with Geomagic *Studio 10 SR1* (64bit), where only a rotation around the z-axis is unrestricted. For each CT data set, finally an actual nominal comparison is calculated with Geomagic *Studio*.
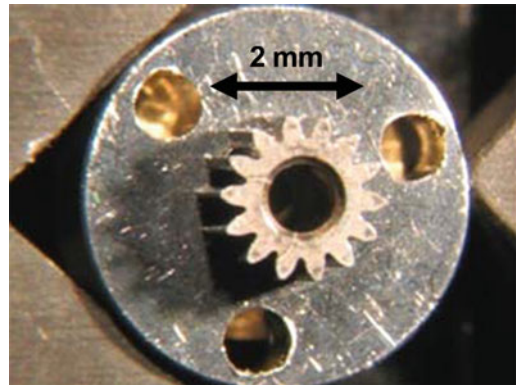

Fig. 12.13 Micro spur-gear with 3 holes on mounting base

The result of the actual nominal comparison is the local difference between the tactile and the CT measurement. This can be interpreted as the measurement error of the CT measurement (see Fig. 12.14).

As a result, a value of 4.8 μm can be a first measure of the measurement uncertainty of micro CT measurements of the micro gear under study. It shows that one voxel measurement uncertainty of micro CT measurement can be achieved even for measurements of sculptured surfaces.

Fig. 12.14 Error of dimension of CT measurement of a micro gear
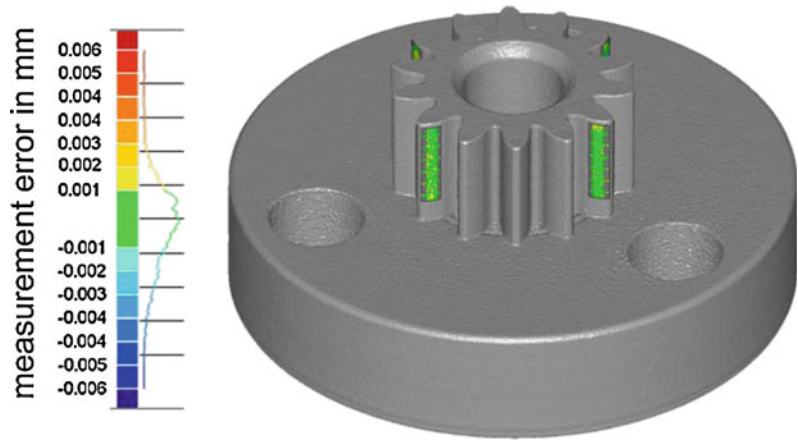
References

1. Buzug, T.M.: Computed Tomography. Springer, Berlin/Heidelberg (2008)
2. Reimers, P., Goebbels, J.: New possibilities of nondestructive evaluation by X-ray computed tomography. Mater. Eval. **41**, 732-737 (1983)
3. Goebbels, J., Illerhaus, B., Onel, Y., Riesemeier, H., Weidemann, G.: 3D-computed tomography over four orders of magnitude 16th world conference on nondestructive testing. Montréal, Canada, Aug 30–Sept 3 2004, CD of Proceedings (2004)
4. Schroer, C.G., Meyer, J., Kuhlmann, M., Benner, B., Günzler, T.F., Lengeler, B., Rau, C., Weitkamp, T., Snigirev, A., Snigireva I.: Nanotomography based on hard x-ray microscopy with refractive lenses. Appl. Phys. Lett. **81**, 1527 (2002)
5. Yin, G.Ch., Tang, M.-T., Song, Y.-F., Chen, F.-R., Liang, K. S., Duewer, F. W., Yun, W., Ko, Ch.-H., Shieh, H.-P.D.: Energy-tunable transmission x-ray microscope for differential contrast imaging with near 60 nm resolution tomography. Appl. Phys. Lett. **88**, 241115 (2006)
6. Rack, A., Zabler, S., Müller, B.R., Riesemeier, H., Weidemann, G., Lange, A., Goebbels, J., Hentschel, M., Görner, W.: High resolution synchrotron-based radiography and tomography using hard X-rays at the BAM*line* (BESSY II). Nucl. Instr. Methods, A **586**, 327–344 (2008)
7. Ewert, U., Robbel, J., Bellon, C., Schumm, A., Nockemann, C.: Digital laminography. International symposium on computerized tomography for industrial applications. DGZfP Berichtsband **44**, 148 (1994)
8. Zhou, J., Maisl, M., Reiter, H., Arnold, W.: Computed laminography for materials testing. Appl. Phys. Lett. **68**, 3500 (1996)
9. Kak, A.C., Slaney, M.: Principles of Computerized Tomographic Imaging. IEEE Press, New York (1987)
10. Feldkamp, L.A., Davis, L.C., Kress, J.W.: Practical cone-beam algorithm. J. Opt. Soc. Am. 1 612–619 (1984)
11. Kalender, W.A., Seissler, W., Klotz, E., Vock, P.: Spiral volumetric CT with single-breath-hold technique, continuos transport and scanner rotation. Radiology **176**, 181–183 (1990)
12. Katsevich, A.: Theoretically exact filtered backprojection-type inversion algorithm for spiral CT. SIAM J. Appl. Math. **62**, 2012–2026 (2002)
13. Hiller, J., Kasperl, S., Schön,T., Schröpfer, S., Weiss, D.: Comparison of probing error in dimensional measurement by means of 3D computed tomography with circular and helical sampling. http://www.ndt.net/article/aero2010/papers/we5a1.pdf
14. Sawicka, B.D., Palmer, B.J.F.: Density gradients in ceramic pellets measured by computed tomography. At. Energy Can. AECL 9261 (1986)
15. Rabe, T., Rudert, R., Goebbels, J., Harbich, K.-W.: Evaluation of green components by nondestructive methods. Ceram. Trans. **133**, 86–95 (2002)
16. Rabe, T., Rudert, R., Goebbels, J., Harbich, K.-W.: Nondestructive evaluation of green components. Am. Ceram. Soc. Bull. **82**(3), 27–32 (2003)
17. Goebbels, J., Weidemann, G., Dittrich, R., Mangler, M., Tomandl, G.: Functionally graded porosity in ceramics—analysis with high resolution computed tomography. Ceram. Trans. **129**, 113–124 (2002)
18. Tomandl, G., Mangler, M., Stoyan, D., Tscheschel, A., Goebbels, J., Weidemann, G.: Characterisation methods for functionally graded materials. J. Mater. Sci. **41**, 4143–4151 (2006)
19. Jasiûniene, E., Illerhaus, B., Goebbels, J.: Use of 3D micro tomography for the investigation of the mechanical properties of cellular metals. In: Green, R.E., Djordjevic, B.B., Hentschel, M.P. (eds.) Nondestructive Characterization of Materials, Springer, Berlin (2003)
20. Engler, P., Friedman, W.D.: Review of dual-energy computed tomography techniques. Mater. Eval. **48**, 623–629 (1990)

21. Ducote, J.L., Alivov, Y., Molloi, S.: Imaging of nanoparticles with dual-energy computed tomography. Phys. Med. Biol. **56**, 2031–2044 (2011)
22. Masad, E.: X-ray computed tomography of aggregates and asphalt mixes. Mater. Eval. **62**, 775–783 (2004)
23. Goebbels, J., Recknagel C., Meinel, D.: Analysis of morphology and composition with computed tomography exemplified at porous asphalt. International Symposium on Digital Industrial Radiology and Computed Tomography (DIR 2007) 25–27 June 2007. Lyon, see: http://www.ndt.net/article/dir2007/papers/27.pdf
24. Nicoletto, G., Anzelotti, G., Konečná, R.: X-ray computed tomography vs. metallography for pore sizing and fatigue of cast al-alloys. Procedia Eng. **2**, 547–554 (2010)
25. Staude, A., Bartscher, M., Ehrig, K., Goebbels, J., Koch, M., Neuschaefer-Rube, U., Noetel, J.: Quantification of the Capability of Micro CT to Detect Defects in Castings Using a New Test Piece and a Voxel-Based Comparison Method. NDT & E International **44**, 531–536 (2011)
26. Staude, A., Krah, T., Goebbels, J., Büttgenbach, S.: Ein dreidimensionaler Prüfkörper für die Lunkererkennung in Gussteilen mittels Computertomographie. Fachtagung Industrielle Computertomographie, proceedings, Shaker, Aachen (2010)
27. Tan, J.C., Elliot, J.A., Clyne, T.W.: Analysis of tomography images of bonded fibrenetworks to measure distributions of fibre segment length and fibre orientation. Adv. Eng. Mater. **8**(6) 495–500 (2006)
28. Robb, K., Wirjadi, O., Schladitz, K.: Fiber orientation estimation from 3d image data: practical algorithms, visualization, and interpretation. IEEE, Proceedings of the 7th International Conference on Hybrid Intelligent Systems, 320–325 (2007)
29. Teßmann, M., Mohr, S., Gayetskyy, S., Haßler, U., Hanke, R.: Automatic determination of fiber-length distribution in composite material using 3D CT data.
EURASIP J. Adv. Sig. Process., S. Article ID 545030 (2010)
30. Mellmann, G., Goebbels, J.: Characterization of fibre reinforced concrete samples by computerized tomography. Poster exhibition. International Conference on Composite Construction, Innsbruck, Innsbruck Austria, 16–18 Sept 1997
31. Falkner, H., Henke, V.: Steel fibre concrete for underwater slabs at potsdamer platz. Struct. Eng. Int. **4**, 238–241 (1997)
32. Weidemann, G., Stadie, R., Goebbels, J., Hillemeier, B.: Computed tomography study of fibre reinforced autoclaved aerated concrete. MP **50**, 278–285 (2008)
33. Beck, M., Goebbels, J., Burkert, A., Isecke, B., Baessler, R.: Monitoring of corrosion processes in chloride contaminated mortar by electrochemical measurements and X-ray tomography. Mater. Corros. **6**, 475–479 (2010)
34. Goebbels, J., Hanke, D., Meinel, D., Staude, A., Beck, M., Burkert, A.: Computed tomography—a new tool studying hidden corrosion. http://www.ndt.net/article/ecndt2010/…/1_09_03.pdf
35. Bartscher, M., Hilpert, U., Goebbels, J., Weidemann, G.: Enhancement and proof of accuracy of industrial computed tomography (CT) measurements. CIRP Ann., Manufact. Technol. **56**(1), 495–498 (2007)
36. Kruth, J.-P., Bartscher, M., Carmignato, S., Schmitt, R., De Chiffre, L., Weckenmann, A.: Computed tomography for dimensional metrology. CIRP Ann., Manufact. Technol. **60**(2), 821 (2011)
37. Bartscher, M., Neukamm, M., Hilpert, U., Neuschaefer-Rube, U., Härtig, F., Kniel, K., Ehrig, K., Staude, A., Goebbels, J.: Achieving traceability of industrial computed tomography. Key Eng. Mater. **437**, 79–83 (2010). http://www.scientific.net/KEM.437.79
38. Neuschaefer-Rube, U., Bartscher, M., Neukamm, M., Neugebauer, M., Härtig, F., Goebbels, J., Ehrig, K., Staude, A.: Measurement of micro gears: comparison of optical, tactile-optical and CT-measurements. Proc. SPIE **7864**, 78640H-1–78640H-9 (2011)